JOIV : Int. J. Inform. Visualization, 6(4) - December 2022 842-849

INTERNATIONAL JOURNAL
ON INFORMATICS VISUALIZATION

journal homepage : www.joiv.org/index.php/joiv

Determining Forest Fire Position from UAV Photogrammetry using Color Filtration Algorithm

Abdul Muid [a,b,*], Maria Evita [b], Nina Aminah [b], Maman Budiman [b], Mitra Djamal [b]

[a] *Department of Physics, FMIPA, Universitas Tanjungpura, Jl. Prof. Dr. Hadari Nawawi, Pontianak 78124, Indonesia*
[b] *Department of Physics, Institut Teknologi Bandung, Jl. Ganesha 10 Bandung 40132, Indonesia*
*Corresponding author: *muid@physics.untan.ac.id*

***Abstract*— Forest fires frequently happen worldwide, especially in the dry season. A forest fire early warning system (EWS) is needed to prevent this disaster. The main part of EWS is the hotspot detection system. On the other side, Unmanned Aerial Vehicle (UAV) technology offers an alternative solution to detect the hotspot for poor satellite image processing accuracy. Remote sensing techniques with UAV working drones are progressively challenging. Drones can provide results in 2D and 3D images with high resolution and real-time. Therefore, in this research, we have used a photogrammetry application from the number of images collected by a UAV with an optimum flight plan for the mission to determine the location of the forest fire. This paper describes remote sensing experiments using drones to detect land fires. The experiment was carried out using a quadcopter drone of the DJI Phantom 4 Pro. The photos are processed using Agisoft Metashape Professional image processing software and become a 2D image. These images captured a fire simulation in a known location. After a high resolution (GSD – Ground Sampling Distance – 0.87cm/px) orthophoto had been generated, a color filtration algorithm detected a hotspot to detect a fire at the exact location. The results are almost zero deviation of longitude and latitude from the real location with 1.44 m^2 and 1.06 m^2 fire area from 2 experiments. This algorithm program has TPR and FPR are 0,78 and 0, respectively. Further research can develop an EWS with a combination of UAV and Wireless Sensor Networks.**

***Keywords*— Unmanned Aerial Vehicle (UAV); forest fires detection; color filter algorithm; high-resolution orthophoto.**

Manuscript received 9 Jun. 2022; revised 4 Aug. 2022; accepted 4 Nov. 2022. Date of publication 31 Dec. 2022.

I. INTRODUCTION

Throughout history, UAVs (Unmanned Aerial Vehicles) have undergone some evolution, contributing to their broad classification range. Recoverable UAVs for remote and automatic control types have gradually become more efficient, higher-performance products and are widely used by different users [1]–[3]. Nowadays, the rapid need for aerial photos acquisition for some applications has changed the direction of UAVs technology growth [4], [5]. These applications are divided into some categories: agriculture (such as analysis of field soil [6], health assessment of crops [7], monitoring crops and irrigation system monitoring [8]), military (such as bomb recognition and military surveillance) [9], architecture-engineering- and construction (AEC) (such as structural and infrastructure inspections [10], transportation [11], cultural heritage conservation, city and urban planning [12]) and civilian (such as photography [13], [14], disaster management [15], [16], archeological survey [17], livestock surveillance [18], safety inspection [19], life observance [20], weather forecasting [21] and geographic mapping [22]).

As one of the categories, photogrammetry has great potential to be applied for some applications, such as forest fire detection [23], [24]. UAVs can be used to measure the canopy of a forest [25]. UAVs can be used to capture field and building mapping instead of satellite imagery [26]. UAVs can fly higher and rapidly survey large areas, and propeller-type UAVs fly at low altitudes to collect high-resolution data for early warning systems [27]. Forest detection analysis has been carried out by Sopholwit Khamphilung from satellite imagery using the CART algorithm [28].

There are two types of drones based on shape, Fixed Wing and Rotary Wings. Rotary Wing is adjusted according to the number of motors or propellers [29]. The helicopter model a copter that only has 1 propeller. Double copter has 2 propellers, usually, the propellers are mounted on both sides of the plane. Tri copter, with 3 propellers and type 4 propellers (quad copter), this type of drone is most widely used today. UAV can be controlled with remote controllers, which are generally equipped with GPS to help the UAV determine its flying position, such as smartphones [30]. UAV is an integrated technology between the use of robot control technology and communication technology. UAV can transmit data from various sensors in remote areas (unreached areas) and are equipped with high-resolution cameras that allow users to monitor a certain location from a height in real-time.

Early detection and monitoring system of forest fires becomes ever more vital as forest fires' incidence increases which is the event in the last decade. Since the early 2000s, an estimated 50,000 fires have occurred yearly in the Mediterranean basin. According to the Mediterranean Forestry Action Program, in 2017, forest fires burned 442,400 hectares of rural and urban areas in Portugal [31]. In Australia, nearly 19 million hectares of forest were burned, more than 3,000 homes were destroyed, and 33 people were killed in the 15,344 bushfires that occurred in 2019 – 2020 [32].

In Indonesia, forest fire frequently happens, especially in August – October [33]. Several studies to predict forest fires have been conducted with many strategies, such as using sensors of temperature, humidity, rainfall [34], watchtowers, satellite, optical sensors, digital cameras [35], light, smoke [36], wind speed, and so on. In the last decade, wireless sensors network (WSN) has been introduced for forest fire prevention [37]. However, the availability of electrical energy is a problem in this regard, considering the forest area is far from an electrical source [38]. Smart systems are needed, such as data collection techniques that are under the conditions in the field. The UAV allows for the retrieval of data and information needed in the event of a forest fire. The UAV can carry various sensors and is equipped with a thermal camera and photo and video cameras [39]. That device can potentially be used to build an early detection system for forest fires [40].

A forest fire early warning system is needed to prevent this disaster, and the main part of this system is the fire detection system. Conversely, unmanned aerial vehicle (UAV) technology offers an alternative solution to detect forest fires for poor satellite image processing accuracy. Therefore, in this research, we have used a photogrammetry application from many images collected by a UAV with an optimum flight plan for forest fire detection analysis using a color filter algorithm.

II. Material and Method

The experiment was conducted on land at Babakan Sari 2 Street, Kiara Condong, Bandung, West Java. That area is ground; parks, agricultural land, and buildings at this location are close to the incinerator, so the potential for land fires to occur during the trash burning is rather high. This study used a quadcopter type of drone, DJI Phantom 4 Pro, with specifications in table I. Drones are used to map and monitor the area from the air. DJI Phantom 4 Pro, with a battery of 5870 mAh and 12 MP camera, has software compatible with Android smartphones was controlling this Phantom 4 Pro with DJI GO software. After the image had been taken by the drone, which flew following the flight plan, they were imported to the software to build 2D model and an orthophoto for further analysis. The color filtration algorithm detected the orthophoto, which had been created in MATLAB to detect a hotspot.

TABLE I
Specification of UAV

Aircraft	
Name	Phantom 4 Pro/Pro+
Type	Quad copter
Version	V2.0
Weight (Battery & Propellers Include)	1388 g
Diagonal Size (Excluding Propellers)	350 mm
Max Speed	45 mph (S-mode) 36mph (A-mode) 31mph (P-mode)
Max Tilt Angle	42° (sport mode) 35° (Attitude mode) 25° (GPS mode)
Max Service Ceiling Above Sea Level	19685 ft (6000m)
Max Wind Speed Resistance	10 m/s
Max Flight Time	Approx. 30 minutes
Operating Temperature Range	32° to 104° F (0° to 40° C)
Gimbal	
Stabilization	3-axis
Controllable Range	Pitch: -90 ° to +90°
Max Controllable Angular Speed	Pitch: 90°/s
Intelligent Flight Battery	
Capacity	5870mAh
Voltage	15.2 V
Battery Type	LiPo 4S
Energy	89.2Wh
Camera	
Sensor	1" CMOS; Effective pixels: 20M
Lens	FOV (Field of View) 84°, 8.8 mm (35 mm format equivalent: 24 mm), f/2.8 - f/11, auto focus at 1 m - ∞
Max. Bitrate of Video	100 Mbps
Photo	JPEG, DNG (RAW) JEP+DNG

Fig. 1 is the hotspot forest fire detection mechanism carried out in this research. A UAV collects images of a known location (-6.922889° latitude, 107.649062° longitude) fire in progress with an optimum flight plan. Fig. 2 is a flight plan installed on a smartphone to make UAV mission for about 3 minutes 30 seconds of 30 m flight altitude in high-speed flight, 70° camera angle, and 90% image overlap. This mission was obtained in 2 successful experiments with a 17-minute interval between the experiment.

Data was imported to Pix4D mapper after geolocation data images, ground control points, and images were collected to get a digital model of the area. Each coordinate of the spots in the images was collected, saved, and compared for image compatibility. A model's orthophoto was generated after point cloud and mesh steps were analyzed for its application. After an orthophoto had been generated, a hotspot was detected by the color filtration algorithm. Fig. 3 is an analysis process to detect a fire and the area of this spot.

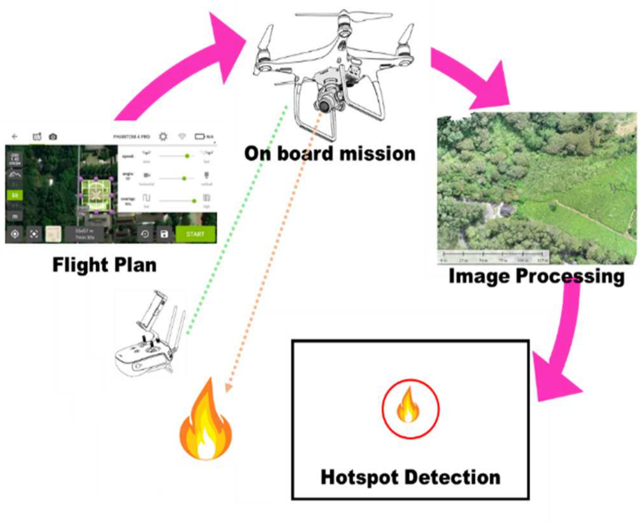

Fig. 1 Mechanism of forest fire detection

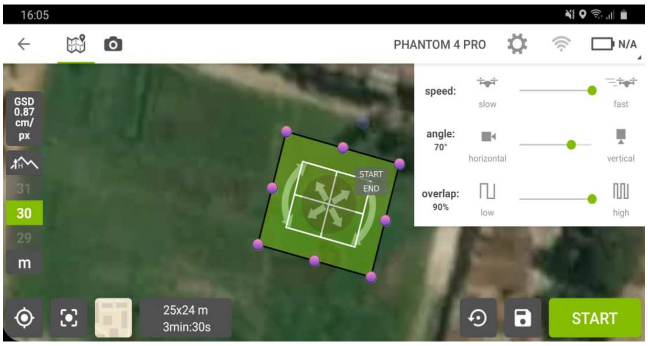

Fig. 2 Flight plan made for UAV mission

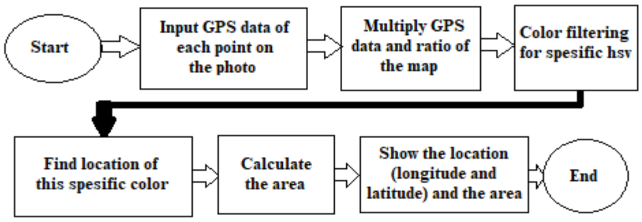

Fig. 3 Process diagram of UAV photogrammetry analysis

III. Result and Discussion

The orthophoto of 2 experiments is presented in Fig. 4 where experiment 1 is on the left and experiment 2 on the right side generated from the digital elevation model (DEM). Fig. 5 is the digital elevation model (DEM) for each experiment. This high-accuracy photo overlaps more than 9 points with more than 3 mean key points for each image and more than 4 million dense point clouds for 15 – 16 thousand points with almost zero reprojection error (Table I). The process took about 65 minutes (Table II) before the hotspot detection.

We use image data processing at a medium level in image processing. Photos are imported and entered into a project on the Agisoft Metashape worksheet. The first process is the align photos process to produce an initial 2D model, as shown in Figure 4. The align photos process report is shown in Table II. The next step is the Dense Point Clouds which is a collection of high points in the number of thousands to millions of points resulting from photogrammetric processing of aerial photos. It takes a total of about 4 hours and 48 minutes. The next process is Build Mesh, one of the main outputs of aerial photo processing in Agisoft Metashape. In comparison, the next process is the Texture Model, which looks at 2D physical models of the features in the photo coverage area.

Fig. 4 Orthophoto generated from UAV capture of experiment 1 (left) and experiment 2 (right)

The aircraft utilizes GPS, a stereo Vision System, and Infrared Sensing System to stabilize, avoid obstacles or track moving subjects. The Vision System uses ultrasound and image data to help the aircraft maintain its current position, enabling precision to hover indoors or in environments where a GPS signal is unavailable. Safety modes include Failsafe and Return-to-Home to ensure the safe return of aircraft if the control signal is lost. When the Forward Vision System is enabled, and lighting conditions are sufficient, the maximum flight attitude angle is 25° with a maximum flight speed of 31 mph (50 kph). The flight controller can also save critical flight data from each flight to the onboard storage device. When forward obstacle sensing is disabled, the maximum flight attitude angle is 35°, and the maximum flight speed is 36 mph (58 kph). The maximum flight speed of the aircraft is increased to 45mph (72kph). Flight data is automatically recorded in the internal storage of the aircraft. This includes flight telemetry, aircraft status information, and other parameters. The data can be accessed by connecting the aircraft to the PC through the Micro USB port.

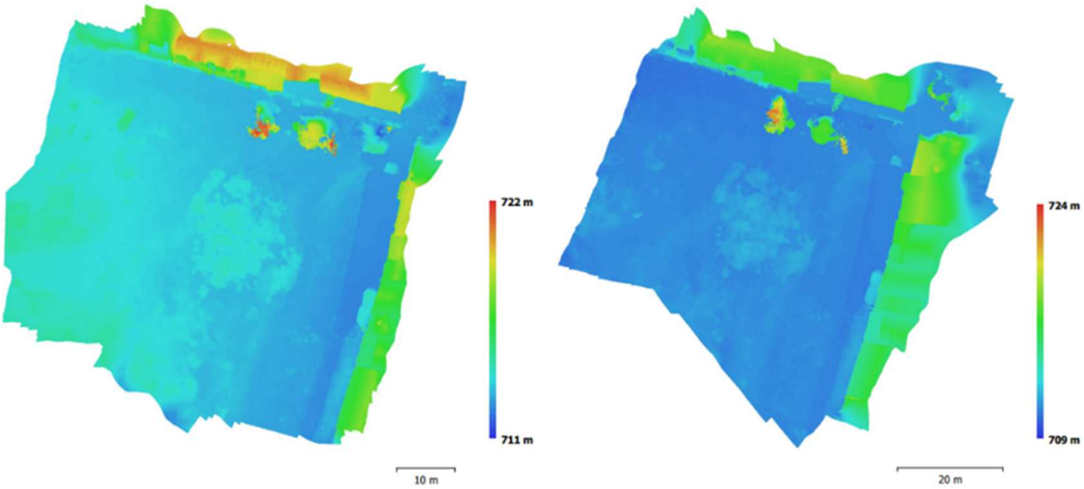

Fig. 5 Digital elevation model (DEM) of UAV capture photo of experiment 1 (left) and experiment 2 (right)

The DJI Phantom 4 Pro is an UAV/drone equipped with a smart flying camera with obstacle sensing made up of vision and infrared sensors, making it able to intelligently autonomous flight. Phantom 4 pro has the best image quality for the Phantom, with greater clarity, lower noise, and higher resolution photos and videos. Dual frequency support in the remote controller makes the HD video downlink more efficient and more stable. The Phantom 4 Pro/Pro+ V2.0 also features a more efficient its propulsion system, as well as a 4dB (60%) operational noise reduction.

DJI GO is an auxiliary software used in experiments because it is compatible with Phantom 4 pro. DJI GO is installed on the smartphone. The Phantom 4 Pro / Pro+ flies anywhere visible on-screen with a tap and tracks moving subjects effortlessly. The Phantom 4 Pro / Pro+, shoots at 4K at up to 60 frames per second. Phantom 4 Pro captures photos that look sharp and clean thanks to the 1-inch CMOS sensor supplementary to the Phantom Pro 4. In addition, Phantom 4 Pro has a 20-megapixel camera resolution. The Phantom 4 pro has an autofocus feature, making it very easy to fly.

TABLE II
SUMMARY OF PHYSICAL PARAMETERS

Parameter	**Experiment 1**	**Experiment 2**
General		
Cameras	42	41
Aligned cameras	42	41
Coordinate system	WGS84 (EPSG:4326)	WGS 84 (EPSG:4326)
Rotation angles	Yaw, Pitch, Roll	Yaw, Pitch, Roll
Point Cloud		
Points	16,074 of 19,475	15,316 of 19,108
RMS reprojection error	0.169685 (0.611975 pix)	0.176714 (0.630372 pix)
Max reprojection error	0.510661 (16.4022 pix)	0.532509 (30.7684 pix)
Points	16,074 of 19,475	15,316 of 19,108
Mean key point size	3.54919 pix	3.37162 pix
Effective overlap	9.45612	9.49445
Alignment parameters		
Accuracy	High	High
Key point limit	40,000	40,000
Tie point limit	4,000	4,000
Dense Point Cloud		
Points	4,337,796	4,288,953
Model		
Faces	15,812	17,063
Vertices	8,119	8,743
Texturing parameters		
Texture size	4,096 x 4,096	4,096 x 4,096
DEM		
Size	2,467 x 2,274	3,227 x 3,255
Orthomosaic		
Size	9,488 x 8,768	10,188 x 9,596

This experiment uses the smartphone-Oppo A3 (4GB RAM and Android 8.1) and the Asus A455L laptop (Intel Core i5, 12 GB RAM based on Windows 10) for the computer. DJI Go 4 version 4.3.20 software is installed on a smartphone for manual flight to evaluate the environment weather, assess the optimal altitude, and inspect other data. DJI Go 4 is also used to control the gimbal, camera, and other aircraft device functions. This application has equipment, an editor, and sky pixel features that can be used to configure the aircraft and edit and share photos and videos. In this software, several indicators on the UAV are informed, such as connectivity between UAV and Android devices, X, Y, and Z positions of the UAV, UAV speed, and remaining battery capacity.

TABLE III
SUMMARY OF PROCESSING TIME

Parameter	**Experiment 1**	**Experiment 2**
Alignment parameters		
Matching time	8 minutes 5 seconds	6 minutes 57 seconds
Alignment time	11 seconds	11 seconds
Dense Point Cloud		

Depth maps generation time	48 minutes 4 seconds	49 minutes 59 seconds
Dense cloud generation time	2 minutes 21 seconds	2 minutes 24 seconds
Model Reconstruction parameters		
Processing time	2 seconds	1 seconds
Texturing parameters		
UV mapping time	26 seconds	18 seconds
Blending time	1 minute 52 seconds	1 minutes 13 seconds
DEM Reconstruction parameters		
Processing time	11 seconds	13 seconds
Orthomosaic Reconstruction parameters		
Processing time	2 minutes 27 seconds	4 minutes 5 seconds

Ground Sampling Distance (GSD) is the distance between 2 center pixels measured on the object's surface. The image with greater GSD has a lower spatial resolution, and less detail can be seen. For example, GSD is 5 cm, so 1 pixel in the image represents an image of 5 x 5 = 25 cm^2 on the object's surface. In this experiment, a flight plan was created using the Pix4D Capture software to conduct 2 flight missions. Each flight covered an area of 52x63 m^2 with an aircraft speed of 10-12 m/sec (fast). The camera angle is 70^o with an overlap of 90%, so the resulting 2D image has a luxurious quality. Overlap determines what percentage of the same part will be re-photographed. The bigger the overlap is better; however, the longer it takes.

Temperature and wind speed around the experimental site were measured before flying the Phantom 4 Pro. This is to ensure the drone's safety while flying and standard operating procedures for drone flights. The average temperature and wind speed around the experimental location are 32.85^o C and 2.95 m/s, respectively, as shown in Figure 6. The wind speed during the experiment was pleasant for flying the drone because the allowed wind speed threshold was less than 10m/s.

A hotspot was detected (Fig. 7) by color filtration algorithm to detect a fire (Fig. 8 - 10) at the exact location (almost zero deviation of longitude and latitude from the real location) from 2 experiments with 1.44 m^2 hotspot area of experiment 1 and 1.06 m^2 of experiment 2 in a location.

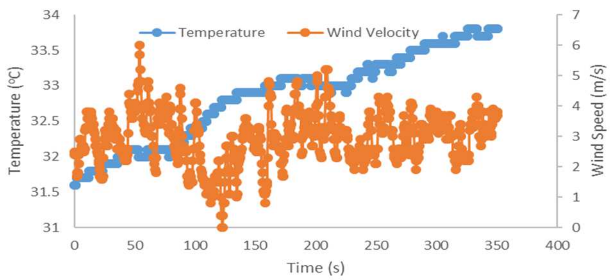

Fig. 6 Temperature (blue graph) and wind speed (orange graph) of experiments.

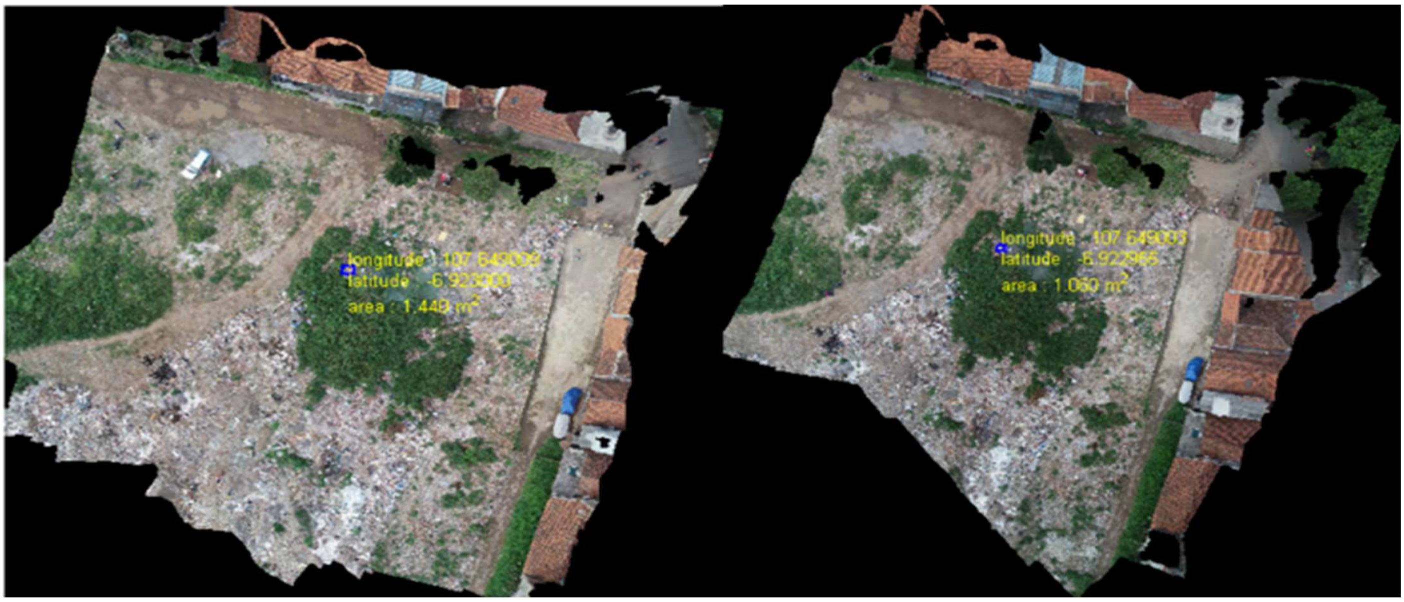

Fig. 7 Hotpot detected at experiment 1 (left) and experimented 2 (right)

In order to locate the hotspot position, color filtration [41], [42] is applied to the image. Depending on the flame's temperature [43], [44], a hotspot color could range from yellow to brownish. This color dynamic is easier to be mapped using HSV [45] color model [46]. Therefore the first step in detecting a hotspot in an image is to convert the image into HSV. In order to detect the fire spot, it is necessary to separate the spot from the background. Fire spot pixels were separated based on their values, saturation, and hue. For instance, this separation could be achieved by masking the image using a certain hue range, such that only pixels with reddish or yellowish color may appear, and the other pixels are hidden. The hue range's lower and upper bounds were determined manually using trial and error. The same goes for saturation and value. Hotspot location in latitude and longitude is obtained by manually fitting four corners of the image into specific longitude and latitude in Google Maps; this process is called georeferencing [47].

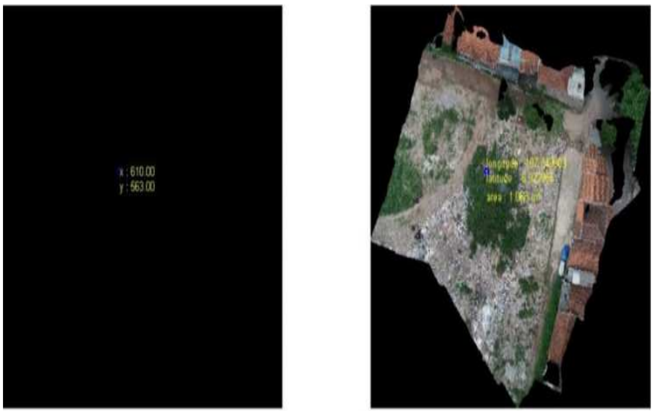

Fig. 8 Filtering process for specific color of fire indication

Fig. 9 Specific colour indicates fire

Fig. 10 The hotspot detected shown by its hue, saturation, and value (left), hotspot location (right)

That information could be used to determine the scale of the image to locate the hotspot position. Two layers of the color filter are made to extract information about a certain hotspot. The first layer has a very narrow hue, saturation, and value range to isolate a certain color that only presents in a hotspot, thus obtaining its position. The next layer is used to find the area of the hotspot. This second layer has a wider hue, saturation, and value range to determine the hotspot area. As illustrated in (1), (2), and (3), an area around a hotspot could vary in color,

$$h = (Ihsv\ (:,:,1) >= 0.001)\ \&\ (Ihsv(:,:,1) <= 0.158) \tag{1}$$

$$s = (Ihsv\ (:,:,2) >= 0.41)\ \&\ (Ihsv(:,:,2) <= 0.415) \tag{2}$$

$$v = (Ihsv\ (:,:,3) >= 0.91)\ \&\ (Ihsv(:,:,3) <= 1) \tag{3}$$

it could range from white to dark brown; all those colors are still part of the fire. These two filter layers could extract information about the hotspot location (latitude and longitude) and hotspot area.

In issues of accuracy and error calculation, we have implemented an assessment to find out how accurately this hotspot detection algorithm program decides to consider an object of color as a fire or not. We have verified in expressions of TPR (True Positive Rate) and FPR (False Positive Rate) values. The algorithm will work to detect hotspots, and the results will be marked with a rectangle which, according to the algorithm, is a hotspot. However, the results detected by the algorithm are not necessarily correct. The algorithm squares the red spots, which are red plastic. In this case, the algorithm produces a false positive (the detection is wrong, we thought it was a fire, even though it was not). Meanwhile, if it is a false negative, it means the algorithm assumes the red points are not fire; it turns out to be a real fire.

We operated this hotspot detection algorithm program on 10 sample photos/images of the land that we carried out previously taken with drones. The 9 images are photos of land with hotspots, and 1 is a photo of land without hotspots. So, in this case, 9 samples are categorized as positive, and 1 sample is categorized as negative. The result shows that the hotspot detection algorithm program decided that 7 of the samples were positive (7 True Positive) and 3 negative, with the basic metrics are TP = 7, FP = 0, TN = 1 and FN = 2, and the advanced metrics are precision = TP/TP+FP = 7/7 = 1, TPR = TP/TP+FN = 7/9 = 0.78 and FPR = FP/FP+TN = 0/1 = 0. The precision and TPR are both very high.

IV. Conclusions

Photogrammetry from a number of images collected by a UAV with an optimum flight plan for the mission has been applied for forest fire hotspot detection. These images captured a fire simulation in a known location. After a high-resolution orthophoto had been generated, a hotspot was detected by color filtration algorithm to detect a fire at the exact location from 2 experiments with 1.44 m^2 hotspot area of experiment 1 and 1.06 m^2 of experiment 2. This algorithm program has TPR and FPR are 0,78 and 0, respectively. This hotspot detection algorithm program can be used to develop an early detection system for forest fires by combining fire detection using ground sensors (WSN) and remote sensing (Satellite) to obtain a trusted early detection system.

Acknowledgment

The authors thank DRPM-RISTEK/BRIN, Ministry of Research and Technology/ Board of National Research and Innovation of Republic of Indonesia for the financial support through the scheme of Doctoral Dissertation Research.

References

[1] S. Darvishpoor, J. Roshanian, A. Raissi, and M. Hassanalian, "Configurations, flight mechanisms, and applications of unmanned aerial systems: A review," *Progress in Aerospace Sciences*, vol. 121. Elsevier Ltd, Feb. 01, 2020. doi: 10.1016/j.paerosci.2020.100694.

[2] C. Xu, X. Liao, J. Tan, H. Ye, and H. Lu, "Recent Research Progress of Unmanned Aerial Vehicle Regulation Policies and Technologies in Urban Low Altitude," *IEEE Access*, vol. 8, pp. 74175–74194, 2020, doi: 10.1109/ACCESS.2020.2987622.

[3] A. S. Saeed, A. B. Younes, C. Cai, and G. Cai, "A survey of hybrid Unmanned Aerial Vehicles," *Progress in Aerospace Sciences*, vol. 98. Elsevier Ltd, pp. 91–105, Apr. 01, 2018. doi: 10.1016/j.paerosci.2018.03.007.

[4] X. Li, J. Tan, A. Liu, P. Vijayakumar, N. Kumar, and M. Alazab, "A Novel UAV-Enabled Data Collection Scheme for Intelligent Transportation System through UAV Speed Control," *IEEE Transactions on Intelligent Transportation Systems*, vol. 22, no. 4, pp. 2100–2110, Apr. 2021, doi: 10.1109/TITS.2020.3040557.

[5] G. J. J. Ducard and M. Allenspach, "Review of designs and flight control techniques of hybrid and convertible VTOL UAVs," *Aerospace Science and Technology*, vol. 118. Elsevier Masson s.r.l., Nov. 01, 2021. doi: 10.1016/j.ast.2021.107035.

[6] S. Das *et al.*, "UAV-Thermal imaging and agglomerative hierarchical clustering techniques to evaluate and rank physiological performance of wheat genotypes on sodic soil," *ISPRS Journal of Photogrammetry and Remote Sensing*, vol. 173, pp. 221–237, Mar. 2021, doi: 10.1016/j.isprsjprs.2021.01.014.

[7] J. Zheng *et al.*, "Growing status observation for oil palm trees using Unmanned Aerial Vehicle (UAV) images," *ISPRS Journal of Photogrammetry and Remote Sensing*, vol. 173, pp. 95–121, Mar. 2021, doi: 10.1016/j.isprsjprs.2021.01.008.

[8] L. Deng, Z. Mao, X. Li, Z. Hu, F. Duan, and Y. Yan, "UAV-based multispectral remote sensing for precision agriculture: A comparison between different cameras," *ISPRS Journal of Photogrammetry and Remote Sensing*, vol. 146, pp. 124–136, Dec. 2018, doi: 10.1016/j.isprsjprs.2018.09.008.

[9] "Spy in the sky," *Nature*, vol. 445, no. 7130, pp. 808–809, 2007, doi: 10.1038/445808a.

[10] N. Michael *et al.*, "Collaborative mapping of an earthquake-damaged building via ground and aerial robots," *Journal of Field Robotics*, vol. 29, no. 5, pp. 832–841, Sep. 2012, doi: https://doi.org/10.1002/rob.21436.

[11] A. Bauranov and J. Rakas, "Designing airspace for urban air mobility: A review of concepts and approaches," *Progress in Aerospace Sciences*, vol. 125, p. 100726, 2021, doi: https://doi.org/10.1016/j.paerosci.2021.100726.

[12] L. G. B. Y. F. R. L. M. K. C. C. K. QUAN Quan, "Low altitude UAV traffic management:An introductory overview and proposal ," *ACTA Aeronauticaet Astronautica Sinica*, vol. 41, no. 1, pp. 23238–023238, 2020.

[13] H. E. Mohamadi, N. Kara, and M. Lagha, "Heuristic-driven strategy for boosting aerial photography with multi-UAV-aided Internet-of-Things platforms," *Engineering Applications of Artificial Intelligence*, vol. 112, p. 104854, 2022, doi: https://doi.org/10.1016/j.engappai.2022.104854.

[14] L. Li *et al.*, "Ultrahigh-resolution boreal forest canopy mapping: Combining UAV imagery and photogrammetric point clouds in a deep-learning-based approach," *International Journal of Applied Earth Observation and Geoinformation*, vol. 107, p. 102686, 2022, doi: https://doi.org/10.1016/j.jag.2022.102686.

[15] J. Wang *et al.*, "Refined micro-scale geological disaster susceptibility evaluation based on UAV tilt photography data and weighted certainty factor method in Mountainous Area," *Ecotoxicology and Environmental Safety*, vol. 189, p. 110005, 2020, doi: https://doi.org/10.1016/j.ecoenv.2019.110005.

[16] F. de Vivo, M. Battipede, and E. Johnson, "Infra-red line camera data-driven edge detector in UAV forest fire monitoring," *Aerospace Science and Technology*, vol. 111, p. 106574, 2021, doi: https://doi.org/10.1016/j.ast.2021.106574.

[17] F. Chiabrando, F. D'Andria, G. Sammartano, and A. Spanò, "UAV photogrammetry for archaeological site survey. 3D models at the Hierapolis in Phrygia (Turkey)," *Virtual Archaeology Review*, vol. 9, no. 18, pp. 28–43, Jan. 2018, doi: 10.4995/var.2018.5958.

[18] X. Li and L. Xing, "Use of Unmanned Aerial Vehicles for Livestock Monitoring based on Streaming K-Means Clustering**This work was supported by the Australian Research Council.," *IFAC-PapersOnLine*, vol. 52, no. 30, pp. 324–329, 2019, doi: https://doi.org/10.1016/j.ifacol.2019.12.560.

[19] T. Umar, "Applications of drones for safety inspection in the Gulf Cooperation Council construction," *Engineering, Construction and Architectural Management*, vol. 28, no. 9, pp. 2337–2360, Jan. 2021, doi: 10.1108/ECAM-05-2020-0369.

[20] S. Sreenath, H. Malik, N. Husnu, and K. Kalaichelavan, "Assessment and Use of Unmanned Aerial Vehicle for Civil Structural Health Monitoring," *Procedia Computer Science*, vol. 170, pp. 656–663, 2020, doi: https://doi.org/10.1016/j.procs.2020.03.174.

[21] V. A. Korolkov, K. N. Pustovalov, A. A. Tikhomirov, A. E. Telminov, and S. A. Kurakov, "Autonomous weather stations for unmanned aerial vehicles. Preliminary results of measurements of meteorological profiles," in *IOP Conference Series: Earth and Environmental Science*, Dec. 2018, vol. 211, no. 1. doi: 10.1088/1755-1315/211/1/012069.

[22] W. Budiharto, E. Irwansyah, J. S. Suroso, A. Chowanda, H. Ngarianto, and A. A. S. Gunawan, "Mapping and 3D modelling using quadrotor drone and GIS software," *Journal of Big Data*, vol. 8, no. 1, p. 48, 2021, doi: 10.1186/s40537-021-00436-8.

[23] V. Sherstjuk, M. Zharikova, and I. Dorovskaja, "3D Fire Front Reconstruction in UAV-Based Forest-Fire Monitoring System," in *2020 IEEE Third International Conference on Data Stream Mining & Processing (DSMP)*, 2020, pp. 243–248. doi: 10.1109/DSMP47368.2020.9204196.

[24] Z. Jiao *et al.*, "A YOLOv3-based Learning Strategy for Real-time UAV-based Forest Fire Detection," in *2020 Chinese Control And Decision Conference (CCDC)*, 2020, pp. 4963–4967. doi: 10.1109/CCDC49329.2020.9163816.

[25] D. A. Umarhadi, P. Danoedoro, P. Wicaksono, P. Widayani, W. Nurbandi, and A. Juniansah, "The Comparison of Canopy Density Measurement Using UAV and Hemispherical Photography for Remote Sensing Based Mapping," in *2018 4th International Conference on Science and Technology (ICST)*, 2018, pp. 1–5. doi: 10.1109/ICSTC.2018.8528670.

[26] A. Zakiyyatuddin, M. Evita, W. Srigutomo, I. Meilano, and M. Djamal, "Geospatial Survey Analysis for 3D Field and Building Mapping using DJI Drone and Intelligent Flight Battery," *Journal of Physics: Conference Series*, vol. 1772, no. 1, p. 012015, 2021, doi: 10.1088/1742-6596/1772/1/012015.

[27] Z. Qiu, X. Chu, C. Calvo-Ramirez, C. Briso, and X. Yin, "Low Altitude UAV Air-to-Ground Channel Measurement and Modeling in Semiurban Environments," *Wireless Communications and Mobile Computing*, vol. 2017, p. 1587412, 2017, doi: 10.1155/2017/1587412.

[28] S. Khamphilung, "Dong Ra Nang National Forest Change Detection using Multi-temporal LANDSAT 7 ETM + Imagery by Using CART Classification: Object-Oriented Approach," *Current Applied Science and Technology*, vol. 21, no. 2, doi: 10.14456/cast.2021.27.

[29] M. Boon, A. Drijfhout, and S. Tesfamichael, "Comparison of a fixed-wing and Multi-rotor UAV for Environmental mapping applications: A case study," *ISPRS - International Archives of the Photogrammetry, Remote Sensing and Spatial Information Sciences*, vol. XLII-2/W6, pp. 47–54, Aug. 2017, doi: 10.5194/isprs-archives-XLII-2-W6-47-2017.

[30] T. Bonny and M. Abdelsalam, "Autonomous Navigation of UAV based on Android Smartphone," *International Journal of Advanced Computer Science and Applications*, Nov. 2019.

[31] "International Handbook on Forest Fire Protection."

[32] A. I. Filkov, T. Ngo, S. Matthews, S. Telfer, and T. D. Penman, "Impact of Australia's catastrophic 2019/20 bushfire season on communities and environment. Retrospective analysis and current trends," *Journal of Safety Science and Resilience*, vol. 1, no. 1, pp. 44–56, 2020, doi: https://doi.org/10.1016/j.jnlssr.2020.06.009.

[33] L. Kiely *et al.*, "Assessing costs of Indonesian fires and the benefits of restoring peatland," *Nature Communications*, vol. 12, no. 1, p. 7044, 2021, doi: 10.1038/s41467-021-27353-x.

[34] P. Cortez and A. Morais, "A Data Mining Approach to Predict Forest Fires using Meteorological Data," Jan. 2007.

[35] A. A. A. Alkhatib, "A Review on Forest Fire Detection Techniques," *International Journal of Distributed Sensor Networks*, vol. 10, no. 3, p. 597368, Mar. 2014, doi: 10.1155/2014/597368.

[36] A. Molina-Pico, D. Cuesta-Frau, A. Araujo, J. Alejandre, and A. Rozas, "Forest Monitoring and Wildland Early Fire Detection by a Hierarchical Wireless Sensor Network," *Journal of Sensors*, vol. 2016, p. 8325845, 2016, doi: 10.1155/2016/8325845.

[37] U. Dampage, L. Bandaranayake, R. Wanasinghe, K. Kottahachchi, and B. Jayasanka, "Forest fire detection system using wireless sensor networks and machine learning," *Scientific Reports*, vol. 12, no. 1, p. 46, 2022, doi: 10.1038/s41598-021-03882-9.

[38] S. Abdullah, S. Bertalan, S. Masar, A. Coskun, and I. Kale, "A wireless sensor network for early forest fire detection and monitoring as a decision factor in the context of a complex integrated emergency response system," in *2017 IEEE Workshop on Environmental, Energy, and Structural Monitoring Systems (EESMS)*, 2017, pp. 1–5. doi: 10.1109/EESMS.2017.8052688.

[39] A. Matese and S. di Gennaro, "Practical Applications of a Multisensor UAV Platform Based on Multispectral, Thermal and RGB High

Resolution Images in Precision Viticulture," *Agriculture*, vol. 8, p. 116, Jul. 2018, doi: 10.3390/agriculture8070116.

[40] M. A. Akhloufi, A. Couturier, and N. A. Castro, "Unmanned aerial vehicles for wildland fires: Sensing, perception, cooperation and assistance," *Drones*, vol. 5, no. 1, Mar. 2021, doi: 10.3390/drones5010015.

[41] N. Ya'acob, M. Syamirza Mohd Najib, N. Tajudin, A. Laily Yusof, and M. Kassim, "Image Processing Based Forest Fire Detection using Infrared Camera," *Journal of Physics: Conference Series*, vol. 1768, no. 1, p. 012014, 2021, doi: 10.1088/1742-6596/1768/1/012014.

[42] K. Poobalan and S. Liew, "Fire detection based on color filters and Bag-of-Features classification," in *2015 IEEE Student Conference on Research and Development (SCOReD)*, 2015, pp. 389–392. doi: 10.1109/SCORED.2015.7449362.

[43] M. Jamali, N. Karimi, and S. Samavi, "Saliency Based Fire Detection Using Texture and Color Features," in *2020 28th Iranian Conference on Electrical Engineering (ICEE)*, 2020, pp. 1–5. doi: 10.1109/ICEE50131.2020.9260659.

[44] M. Hasan, R. Zaman Khan, N. A. Ibraheem, M. M. Hasan, R. Z. Khan, and P. K. Mishra, "ARPN Journal of Science and Technology:: Understanding Color Models: A Review," *ARPN Journal of Science and Technology*, vol. 2, no. 3, 2012, [Online]. Available: http://www.ejournalofscience.org

[45] Beck K, "Colour fire hot," https://sciencing.com/colours-fire-hot-8631323.html., Feb. 18, 2021.

[46] Ettling B. V., "Colours of smoke and flame," *Fire Arson Investig., vol. 30*, 1980. , https://www.ojp.gov/ncjrs/virtual-library/abstracts/colors-smoke-and-flame (accessed Feb. 02, 2021).

[47] A. Hackeloeer, K. Klasing, J. M. Krisp, and L. Meng, "Georeferencing: a review of methods and applications," *Ann GIS*, vol. 20, no. 1, pp. 61–69, Jan. 2014, doi: 10.1080/19475683.2013.868826.